High-Resolution Measurements of $e^+ + H_2O$ Total Cross Section

A. Loreti,[1] R. Kadokura,[1] S. E. Fayer,[1] Á. Kövér,[2] and G. Laricchia[1,*]
[1]UCL Department of Physics and Astronomy, University College London, Gower Street, London, WC1E 6BT, United Kingdom
[2]Institute for Nuclear Research of Hungarian Academy of Science, Debrecen, PO Box 51, H-4001, Hungary
(Received 20 September 2016; published 16 December 2016)

Using a purely electrostatic positron beam, the total cross section of positrons scattering from H_2O has been measured for the first time with a high angular discrimination ($\simeq 1°$) against forward scattered projectiles. Results are presented in the energy range (10–300) eV. Significant deviations from previous measurements are found which are, if ascribed entirely to the angular acceptances of various experimental systems, in quantitative accord with *ab initio* theoretical predictions of the differential elastic scattering cross section.

DOI: 10.1103/PhysRevLett.117.253401

While the apparent imbalance between matter and antimatter in the Universe remains a major puzzle in science [1,2], much progress in the understanding of the interactions between the two has been achieved through studies of controlled collisions of positrons (e^+) and positronium (Ps, the short-lived atom made of an electron and a positron) with atoms and molecules [3–7].

At low energies, the static and polarization interactions tend to cancel for positrons reducing their scattering probability in comparison with electrons. However, polarization often enhances direct ionization by positrons, so that they can be more penetrating and more ionizing than electrons, a result of potential import in analyses of astrophysical (e.g., [8]) and atmospheric events (e.g., [9]) as well as in positron-track simulations for dosimetry in positron emission tomography (e.g., [10]). In turn, these studies contribute to the motivation for investigating the interaction of e^+ with water which accounts for about 60% of the human body and which is the most abundant greenhouse gas in the atmosphere.

Measurements of positron-water total cross section (σ_T) were first carried out 30 years ago [11,12]. Since then, only a few new results have been added, experimentally [13–15] and theoretically [16,17], without a satisfactory agreement emerging among them. The integral (σ_{el}) and differential ($d\sigma_{el}/d\Omega$) elastic (el) scattering cross sections for $e^+ + H_2O$ have also been measured recently [17], complementing theoretical determinations [18,19].

Because of the long-range forces involved in the scattering of charged projectiles from a polar molecule such as H_2O, one of the major difficulties in measuring σ_T (even in the case of electrons, e.g., [20–23]) lies in discriminating against the considerable flux of small forward-angle scattered particles (FSPs) (e.g., [16,19]). The largest error associated with FSPs arises from elastic scattering and rovibrational inelastic processes which cannot be easily distinguished from the incident flux via energy loss discrimination since this is smaller than (or comparable to) typical beam energy resolutions (e.g., the first vibrational excitation from the ground state $J = 0$ is $\simeq 1595$ cm^{-1} [24]). Detection of FSPs leads to a systematic underestimate of the beam attenuation and, thus, the measured total cross sections. In this respect, beams that employ magnetic fields are more likely to transport FSPs from the interaction region to the detector, with a dependence of σ_T upon the magnetic field strength persisting even for weak fields (e.g., $\simeq$4–9 Gauss [11,12]). This type of systematic effect can be reduced by using electrostatic beams which enable both the interaction and detection regions to be field free, thus, facilitating the attainment of a smaller (energy-independent) angular acceptance [25–27].

For targets with a low polarizability, α (e.g., $\simeq$1.38 a.u. for He), FSPs effects are small (e.g., [25]). However, in the case of H_2O ($\alpha \simeq 9.8$ a.u. and permanent dipole moment, $d \simeq 1.85$ D), they are expected to result in large errors [16,19], e.g., $\simeq$100% of the measured σ_T at 10 eV [28]. In order to remedy this, theoretical $d\sigma_{el}/d\Omega$, in conjunction with the experimental angular resolutions, are routinely employed to compute the FSPs contribution and to correct the measured σ_T [15,17,28].

In this Letter, we present σ_T for $e^+ + H_2O$ measured for the first time with a fully electrostatic positron beam characterized by an angular discrimination against FSPs of $\simeq 1°$. The total cross sections have been measured in the energy range (10–300) eV. The lower limit is just below the first ionization threshold $E_i = 12.62$ eV and slightly above the Ps formation threshold, $E_{Ps} = 5.82$ eV.

The equipment used for this experiment has been described previously [29]. Briefly, positrons from a ^{22}Na source are moderated by a stack of three annealed tungsten meshes (20 μm wire and 70% transmission) [30]. A set of primary lenses transports the beam at 3 keV from the moderator and focuses it to a small beam spot ($R \sim 1$ mm) at the remoderator. This is an annealed W(100) foil (thickness $\simeq$50 nm) with a measured remoderation efficiency of 0.1 [29]. The remoderator (rm) is floated at a

potential ($V_{\rm rm}$) to accelerate the positrons to the required beam energy ($E_+ = eV_{\rm rm} + |\phi|$), where $\phi = -2.7 \pm 0.1$ eV is the positron work function for the current remoderator [29], and e is the elementary charge. The positrons are then transported around a 90° bend through a cylindrical mirror analyzer before reaching the interaction region. Here, an aluminium cylindrical cell is situated of length = 53 mm, inner radius = 25.4 mm, and aperture radius = 0.5 mm [25]. A position sensitive detector (PSD) terminates the flight path. In front of the detector, two grids are mounted that enable retarding potential analysis. The inner grid is also used, during the total cross section measurements, to reflect inelastically forward scattered particles and to bias the beam off during the background measurements, as explained later.

The beam has an angular divergence of 1° and an energy spread of 1% of E_+ [29]. During the course of the current work, beam rates were $(0.02–1.5)e^+s^{-1}$ in the energy range (10–300) eV.

The angular acceptance (θ) for FSPs is energy independent. It is set by geometrical constraints and can be varied by selecting appropriate regions of interest within the beam spot at the PSD. If we consider the cell-to-detector distance $D \simeq 130$ mm, we can define $\theta = \arctan(R_b/D) \simeq 1°$, where R_b is the beam spot radius at the PSD, typically ($\simeq$2 mm).

The total cross section is determined by measuring the attenuation of the beam through the scattering cell containing water vapor. If I_0 and I are, respectively, the incident and transmitted (unscattered) beam intensities, the total cross section is simply given by the Beer-Lambert law

$$\sigma_T = \frac{k_B T}{Pl} \ln\left(\frac{I_0}{I}\right), \tag{1}$$

where P and T are the target gas pressure and temperature, respectively, l is the length of the positron path through the gas and k_B the Boltzmann constant. The temperature was (291 ± 1) K, the pressure was measured by a capacitance manometer (MKS 627D Baratron) temperature stabilized to 45 °C. Thermal transpiration corrections ($\simeq$3.5%) have been applied using the method of [31] with the parameters for H_2O of [32]. The gas flow into the cell was controlled by an electric valve; typical cell pressures were around (0.1–0.4) Pa. During the I_0 runs, a second valve was used to introduce gas directly into the system, bypassing the cell in order to maintain the same background pressure conditions of $\simeq 2 \times 10^{-7}$ mbar throughout the I_0 and I runs.

The measurements were carried out by alternating a run with gas introduced into the cell and a run with gas admitted through the bypass valve. A pause of 30 minutes, with both valves shut, allowed the cell and the system to be evacuated before a new run was started. Before recording the gas run, a wait of 15 minutes was imposed to let the

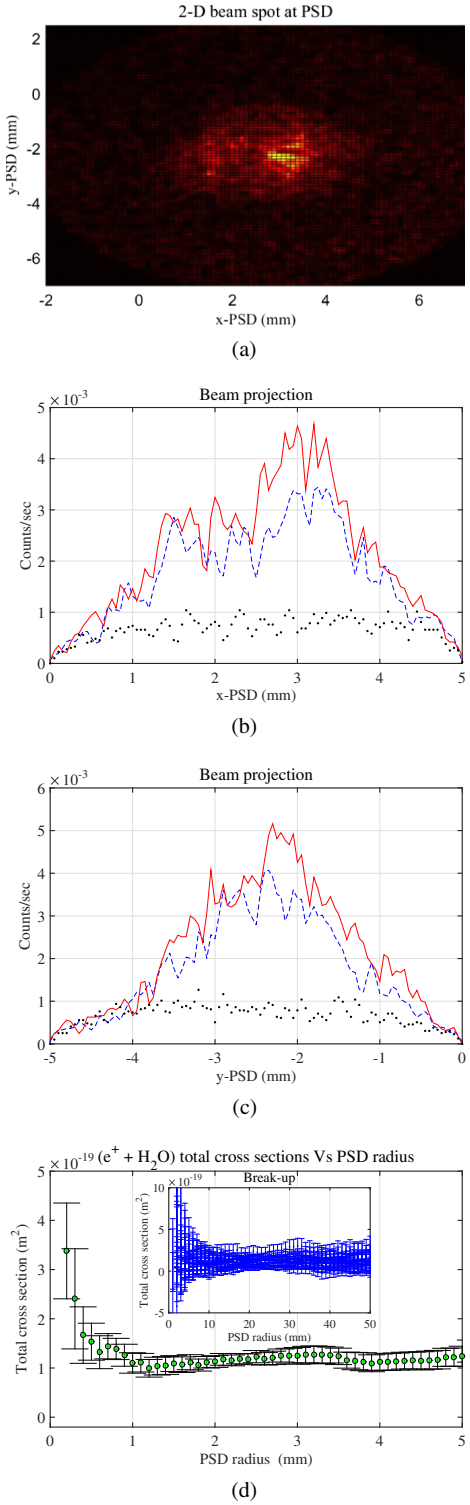

FIG. 1. (a) example of 2D image of the beam spot as seen at the PSD; (b) and (c) beam spot projections on PSD x axis and y axis: (red continuous line) I_0 run, (blue dashed line) I run, (black dots) background. From this kind of plot, the beam center is extracted as explained in the text. (d) Example of the radial dependence of the total cross section for $e^+ + H_2O$ scattering at 30 eV (green bullets, main figure), obtained by averaging the set of total cross section measurements (blue bullets, inset).

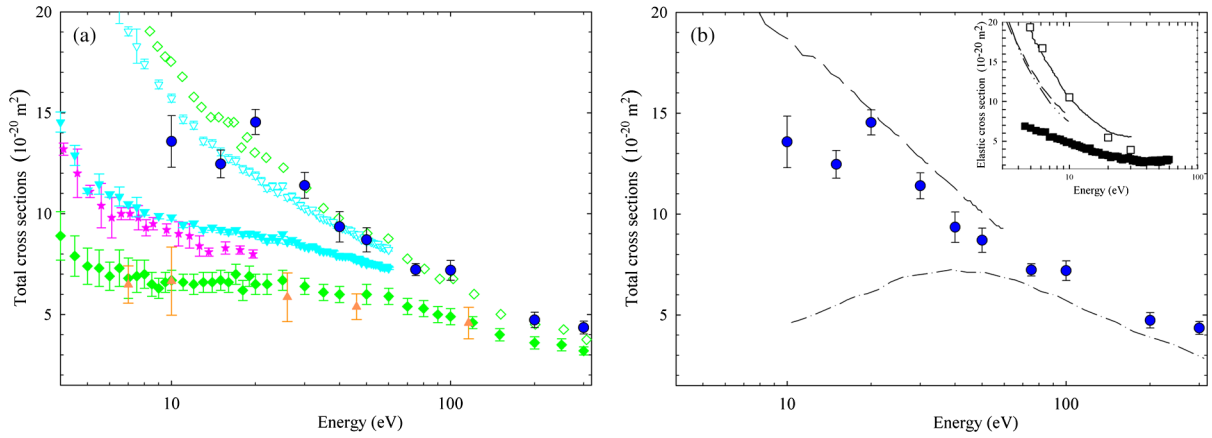

FIG. 2. Cross sections for positron scattering from H_2O. In all cases, solid symbols denote direct measurements, hollow symbols denote measurements corrected for forward-angle elastic scattering, and lines denote theories. (a) σ_T comparison among experiments: filled circle, current work; inverted filled triangle, inverted open triangle, Makochekanwa *et al.* [15]; filled diamond, open diamond, Sueoka *et al.* [11,28]; filled star, Zecca *et al.* [13]; filled triangle, Beale *et al.* [14]. (b) present σ_T results compared with theories: (dashed-dotted line) SCOP [16]; (long dashed line) IAM-SCAR [17]. Inset: σ_{el}: filled square, open square, Tattersall *et al.*, [17]; (short dashed line) R matrix [18], (dashed-double dotted line) [19] close coupling single center, (solid line) R matrix [17,33].

pressure stabilize in the cell. During this wait, a background run was started by applying to the inner grid a potential $\simeq$9 V above V_{rm}. This enabled multiple background acquisitions throughout the whole run. The same grid was biased at V_{rm} during the beam-on measurements in order to repel inelastically scattered particles.

The PSD at the end of the beam line allows for 2D imaging of the beam spot as seen in Fig. 1(a). The center was found by analyzing the projection of the beam spot on the x and y axes, as in Figs. 1(b) and 1(c). The $Q^{(i)}$ coordinate of the center is calculated as

$$Q^{(i)} = \sum_j g_j^{(i)} q_j^{(i)} \qquad i = x, y, \tag{2}$$

where $g_j^{(i)}$ is the rate (after background subtraction) at the $q_j^{(i)}$ coordinate.

In order to extract the total cross section, the beam rates were computed by summing the number of events in concentric disks of increasing radii around the center of the beam spot on the PSD. This analysis yields a radial profile of the beam rates and, hence, of the total cross section, as seen in Fig. 1(d). The total cross section radial profile shows large error bars at small radii mainly due to the low count rate within small sized domains. However, in addition to this statistical uncertainty, potential systematic errors may arise from a possible mismatch between the beam center for the I_0 and I runs which would be more significant at small radii. In the current work, the radius yielding the minimal statistical error on σ_T has been retained as the beam radius. This generally agrees well with the radius extracted from the intensity radial profiles [25].

The current results for the total cross sections of $e^+ + H_2O$ are displayed in Fig. 2 together with (a) earlier experimental and (b) theoretical determinations. Previous results for the elastic scattering cross sections are shown in the inset of Fig. 2(b). In all cases, the direct measurements are illustrated as solid symbols, those corrected for FSPs effects (using various theoretical $d\sigma_{el}/d\Omega$ and experimental angular resolutions as in the original works) are shown as hollow symbols.

Considering the direct measurements of σ_T first, the discrepancy between the present and previous determinations [11,13–15] is evident across the whole energy range; for instance the current measurement being a factor of 1.4–2 higher at 10 eV. Two theoretical predictions of σ_T are shown in Fig. 2(b). The spherical complex optical potential (SCOP) [16] employed an isotropic complex potential to describe the interaction between positron and water molecule, the imaginary component of the potential chosen of the same form as for electrons and empirically scaled using e^+ data. The independent atomic model (IAM) [17] calculated the scattering amplitudes for each of the atoms independently using the optical potential theory, then adding them in order to obtain σ_T for the molecule. The internal structure of the molecule was considered by applying the screen corrected additive rule (SCAR), previously used to calculate electron-molecule scattering with good accuracy in the energy range (10–1000) eV (e.g., [34,35]) and, more recently, adapted to describe positron-molecule scattering [17,36,37]. The model does not include vibrational and rotational cross sections, which have been calculated using the first Born approximation. Our direct measurements display a similar energy dependence to the results of the SCOP calculation above 50 eV and to the IAM-SCAR results above 30 eV, consistently with the expected range of validity of each theory [16,17]. In these ranges, the measurements are, respectively, $\simeq$20% higher and $\simeq$15% lower than the theories.

TABLE I. Angular acceptance θ and corresponding total cross section measurements at 10 eV. The errors deriving from FSPs, $\Delta = 2\pi \int_0^\theta (\sin(\theta')d\sigma_{el}/d\Omega)d\theta'$ are calculated using the theoretical differential elastic scattering cross section of [33]. (The angular acceptance of [11] has not been found in the literature).

Experiment	θ	$\sigma_T \times 10^{-20}$ [m^2]	$\Delta \times 10^{-20}$ [m^2]
Current work	1°	13.6	0.9
Zecca *et al.*, [13]	6°	9.2	4.0
Makochekanwa *et al.*, [15]	7°	9.8	4.3
Beale *et al.*, [14]	12°	6.7	5.2

Also depicted in Fig. 2(a) are the σ_T obtained in [11] and corrected by [28] using the theoretical electron-water $d\sigma_{el}/d\Omega$ of [38]. For positrons, elastic scattering cross sections have been calculated using *ab initio* methods, namely, a close coupling single center approach [19] and a (rotationally summed) *R*-matrix method [18,33]. In the latter, a correction was applied (via the first Born approximation) to account for the large angular momentum terms involved in the long range dipole interaction [18,33]. The correction was not needed in the close coupling single center method as many partial wave terms were directly included in the wave function expansion yielding a convergence of the series [19]. As displayed in the inset of Fig. 2(b), the predictions of the two theories are close. The only measurement of $\sigma_{el}(e^+)$ [17] is also included in the figure and is consistent with theory [17,33] after applying FSPs corrections of, e.g., ≃200% at 5 eV [17]. Makochekanwa *et al* [15] corrected their σ_T measurements using the theoretical $d\sigma_{el}/d\Omega$ of [39]. Both sets of corrected σ_T results [15,28] are seen to be in broad agreement with the present direct measurements. In fact, at 10 eV, where the range of validity of the *R*-Matrix theory [33] overlaps the range investigated in the present work, the deviations among the various measurements are entirely resolved if allowance is made for FSPs effects using the angular resolutions of the experimental systems and the theoretical predictions of $d\sigma_{el}/d\Omega$ [33], as computed in Table I and illustrated in Fig. 3. This implies that, at this energy, elastic scattering accounts for $(\sigma_{el}/\sigma_T) \simeq 80\%$ of all collision processes.

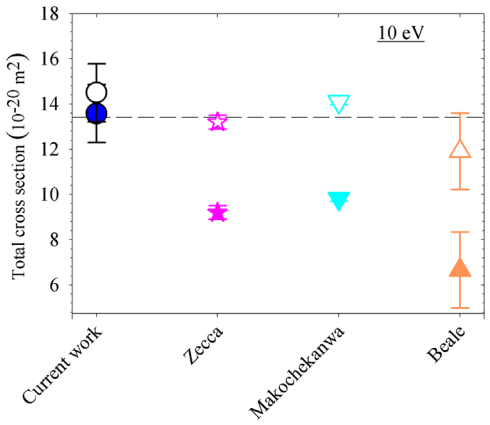

FIG. 3. Comparison of experimental σ_T at 10 eV before (solid symbols) and after (hollow symbols) applying the corrections in Table I. (The errors for the corrected results are those for the direct measurements). Simple mean of the corrected set dashed line (13.4 ± 0.7)Å^2.

In conclusion, the total cross section of $e^+ + H_2O$ has been measured, for the first time, in field-free interaction and detection regions in the energy range (10–300) eV. The high angular discrimination of the current experiment (≃1°) greatly reduces the systematic errors arising from forward scattered projectiles enabling, for the first time, a direct comparison with theories. The experiment has yielded values 50%–100% higher than previous measurements, in quantitative agreement with theoretical predictions in their range of validity. Further high-resolution measurements of σ_T and first $d\sigma_{el}/d\Omega$ $(\theta \leq 10^o)$ are planned.

The data supporting this publication are available at UCL Discovery at [40].

We would like to thank Safe Khan and Lewis Miller for their assistance in the early stages of this project, J. Tennyson and K. L. Balujia for providing tables of their data and useful discussions, Rafid Jawad and John Dumper for excellent technical expertise, Engineering and Physical Sciences Research Council (EPRSC) for financial support (Grants No. EP/E053521/1 and No. EP/P009395/1) and providing support to S. E. F.. A. K. thanks the Hungarian Scientific Research Foundation (OTKA Grant No. K104409).

*g.laricchia@ucl.ac.uk

[1] M. Dine and A. Kusenko, Origin of the matter-antimatter asymmetry, Rev. Mod. Phys. **76**, 1 (2003).
[2] L. Willmann and K. Jungmann, Matter-antimatter asymmetry–aspects at low energy. Ann. Phys. (Berlin) **528**, 108 (2016).
[3] M. Charlton and J. W. Humberston, *Positron physics* (Cambridge University Press, Cambridge, England, 2001), pp. 108–114.
[4] C. M. Surko, G. F. Gribakin, and S. J. Buckman, Low-energy positron interactions with atoms and molecules, J. Phys. B **38**, R57 (2005).
[5] G. Laricchia, S. Armitage, Á. Kövér, and D. J. Murtagh, Ionizing collisions by positrons and positronium impact on the inert atoms, Adv. At. Mol. Opt. Phys. **56**, 1 (2008).
[6] G. Laricchia and H. R. J. Walters, Positronium collision physics, Riv. Nuovo Cimento **35**, 305 (2012).
[7] Y. Nagashima, Experiments on positronium negative ions, Phys. Rep. **545**, 95 (2014).
[8] T. Siegert, R. Diehl, G. Khachatryan, M. G. H. Krause, F. Guglielmetti, J. Greiner, A. W. Strong, and X. Zhang, Gamma-ray spectroscopy of positron annihilation in the milky way, Astron. Astrophys. **586**, A84 (2016).

[9] C. Kohn and U. Ebert, Calculation of beams of positrons, neutrons, and protons associated with terrestrial gamma ray flashes, J. Geophys. Res. **120**, 1620 (2015).
[10] F. Blanco *et al.*, Scattering data for modelling positron tracks in gaseous and liquid water, J. Phys. B **49**, 145001 (2016).
[11] O. Sueoka, S. Mori, and Y. Katayama, Total cross sections for electrons and positrons colliding with H_2O molecules, J. Phys. B **19**, L373 (1986).
[12] O. Sueoka, S. Mori, and Y. Katayama, Total cross sections for positron and electron collisions with NH_3 and H_2O molecules, J. Phys. B **20**, 3237 (1987).
[13] A. Zecca, D. Sanyal, M. Chakrabarti, and M. J. Brunger, Positron scattering from water, J. Phys. B **39**, 1597 (2006).
[14] J. Beale, S. Armitage, and G. Laricchia, Positronium and positron H_2O total cross sections, J. Phys. B **39**, 1337 (2006).
[15] C. Makochekanwa, A. Bankovic, W. Tattersall1, A. Jones, P. Caradonna, D. S. Slaughter, K. Nixon, M. J Brunger, Z. Petrovic, J. P. Sullivan, and S. J Buckman, Total and positronium formation cross sections for positron scattering from H_2O and HCOOH, New J. Phys. **11**, 103036 (2009).
[16] K. L. Baluja and A. Jain, Total (elastic and inelastic) scattering cross sections for several positron-molecule systems at 10–5000 eV: H_2, H_2O, NH_3, CH_4, N_2, CO, C_2H_2, O_2, SiH_4, CO_2, N_2O, and CF_4, Phys. Rev. A **45**, 7838 (1992).
[17] W. Tattersall, L. Chiari, J. R. Machacek, E. Anderson, R. D. White, M. J. Brunger, S. J. Buckman, G. Garcia, F. Blanco, and J. P. Sullivan, Positron interactions with water total elastic, total inelastic, and elastic differential cross section measurements, J. Chem. Phys. **140**, 044320 (2014).
[18] K. L. Baluja, R. Zhang, J. Franz, and J. Tennyson, Low-energy positron collisions with water: elastic and rotationally inelastic scattering, J. Phys. B **40**, 3515 (2007).
[19] F. A. Gianturco, T. Mukherjee, and A. Occhigrossi, Computing positron annihilation in polyatomic gases: An exploratory study, Phys. Rev. A **64**, 032715 (2001).
[20] M. A. Khakoo, H. Silva, J. Muse, M. C. A. Lopes, C. Winstead, and V. McKoy, Erratum: Electron scattering from H_2O: Elastic scattering, Phys. Rev. A **87**, 049902(E) (2013).
[21] H. Silva, J. Muse, M. C. A. Lopes, and M. A. Khakoo, Low Energy Elastic Differential Electron Scattering from H_2O, Phys. Rev. Lett. **101**, 033201 (2008).
[22] A. Faure, J. D. Gorfinkiel, and J. Tennyson, Electron-impact rotational excitation of water, Mon. Not. R. Astron. Soc. **347**, 323 (2004).
[23] A. Faure, J. Gorfinkiel, and J. Tennyson, Low-energy electron collisions with water: Elastic and rotationally inelastic scattering, J. Phys. B **37**, 801 (2004).
[24] O. L. Polyansky, R. I. Ovsyannikov, A. A. Kyuberis, L. Lodi, J. Tennyson, and N. F. Zobov, Calculation of rotationvibration energy levels of the water molecule with near-experimental accuracy based on an *ab initio* potential energy surface, J. Phys. Chem. **117**, 9633 (2013).
[25] S. E. Fayer, A. Loreti, S. L. Andersen, Á. Kövér, and G. Laricchia, Magnetic field-free measurements of the total cross section for positrons scattering from helium and krypton, J. Phys. B **49**, 075202 (2016).
[26] K. Nagumo, Y. Nitta, M. Hoshino, H. Tanaka, and Y. Nagashima, Measurements of total cross sections for positron scattering from He under magnetic-field-free conditions using an electrostatic high-brightness slow positron beam system, J. Phys. Soc. Jpn. **80**, 064301 (2011).
[27] K. Nagumo, Y. Nitta, M. Hoshino, H. Tanaka, and Y. Nagashima, Magnetic-field-free measurements of the total cross sections for positron scattering from neon, Eur. Phys. J. D **66**, 81 (2012).
[28] M. Kimura, O. Sueoka, A. Hamada, and Y. Katayama, A comparative study of electron- and positron- polyatomic molecule scattering, Adv. Chem. Phys. **11**, 537 (2000).
[29] Á. Kövér, A. I. Williams, D. J. Murtagh, S. E. Fayer, and G. Laricchia, An electrostatic brightness-enhanced timed positron beam for atomic collision experiments, Meas. Sci. Technol. **25**, 075013 (2014).
[30] A. I. Williams, D. J. Murtagh, S. E. Fayer, S. L. Andersen, J. Chevallier, A. Kövér, P. Van Reeth, J. W. Humberston, and G. Laricchia, Moderation and diffusion of positrons in tungsten meshes and foils, J. Appl. Phys. **118**, 105302 (2015).
[31] T. Takaishi and Y. Sensui, Thermal transpiration effect of hydrogen, rare gases and methane, Trans. Faraday Soc. **59**, 2503 (1963).
[32] I. Yasumoto, Thermal transpiration effects for gases at pressures above 0.1 Torr, J. Phys. Chem. **84**, 589 (1980).
[33] J. Tennyson (private communication).
[34] F. Blanco and G. Garcia, Screening corrections for calculation of electron scattering from polyatomic molecules, Phys. Lett. A **317**, 458 (2003).
[35] F. Blanco and G. Garcia, Screening corrections for calculation of electron scattering differential cross sections from polyatomic molecules, Phys. Lett. A **330**, 230 (2004).
[36] L. Chiari, A. Zecca, S. Girardi, E. Trainotti, G. Garcia, F. Blanco, R. P. McEachran, and M. J. Brunger, Positron scattering from O_2, J. Phys. B **45**, 215206 (2012).
[37] A. G. Sanz, M. C. Fuss, F. Blanco, Z. Man, J. D. Gorfinkiel, R. P. McEachran, M. J. Brunger, and G. Garcia, Cross-section calculations for positron scattering from pyrimidine over an energy range from 0.1 to 10000 eV, Phys. Rev. A **88**, 062704 (2013).
[38] Y. Okamoto, K. Onda, and Y. Itikawa, Vibrationally elastic cross sections for electron scattering from water molecules, J. Phys. B **26**, 745 (1993).
[39] J. Tennyson (private communication).
[40] See https://dx.doi.org/10.14324/000.ds.1529854.